

A statistical reconstruction algorithm for positronium lifetime imaging using time-of-flight positron emission tomography

Zheyuan Zhu, Charles W. Harrison, Chien-Min Kao, and Hsin-Hsiung Huang

Abstract—Positron emission tomography (PET) has been widely used for the diagnosis of serious diseases including cancer and Alzheimer’s based on the uptake of radiotracers that target diseases’ pathological signatures. Recently, positronium lifetime imaging (PLI) with time-of-flight (TOF) PET can provide supplemental information reflecting conditions of the tissue microenvironment via mechanisms that are independent of tracer uptake. However, the present TOF PET systems have a finite coincidence resolving time (CRT), and the PLI reconstruction problem has yet to be fully formulated for the development of accurate reconstruction methods. This work addresses this challenge by developing a statistical model for the PLI data and deriving from it a maximum-likelihood image reconstruction method for the lifetime image. The proposed lifetime reconstruction method does not require prior knowledge of the radiotracer distribution, nor direct measurement of the time delay between prompt gamma and annihilation photons. Simulation studies have shown that quantitatively correct lifetime images can be reconstructed for phantoms >20 centimeters in diameter at millimeter-scale spatial resolution, which exceeds the resolution limit imposed by the system CRT.

Index Terms—Positron emission tomography, time-of-flight, positronium lifetime imaging, maximum likelihood estimation.

I. INTRODUCTION

The physics that enables positronium lifetime imaging (PLI) with time-of-flight (TOF) positron emission tomography (PET) has recently been elucidated, and the feasibility of PLI has been experimentally demonstrated [1], [2], [3]. PET is widely used for revealing the functional state of an organ or tissue by the uptake of a specific PET molecule as governed by its physiological and biochemical interactions with the body. On the other hand, PLI measures the lifetime of positronium, which is an electron-positron pair formed by a positron released by a PET molecule [4]. Interactions between positronium and paramagnetic molecules such as the oxygen present in the nearby environment shorten its lifetime. Therefore, the positronium lifetime can quantitatively reflect the presence and concentration of such molecules in the microenvironment independent of the uptake mechanism of the PET molecule. This is of clinical interest because, for example, hypoxic tumors are known to be resistant to many therapeutics and knowing the local oxygen concentration may lead to better treatment outcomes. Also, PLI could open the door for the creation of novel contrast mechanisms for PET.

Presently, PLI is demonstrated under the assumption of perfect TOF resolution so that events can be precisely localized to their origins in space. However, current TOF PET systems have a TOF resolution in the range of 200 - 600 ps FWHM,

corresponding to a spatial resolution of 3-9 cm. For such systems, the naive reconstruction methods using the most likely positions (backprojection, BP) based on TOF yield PLI images that have poor resolution and are likely to be quantitatively incorrect. Therefore, PLI reconstruction under limited TOF resolution is an emerging topic of interest.

Incorporating the statistics of the PLI list-mode events could potentially resolve the lifetime image beyond the native TOF resolution. However, this idea has so far only been demonstrated with a rather simplified imaging process [5]. For example, the lifetime measurements do not include the effects of the finite coincidence resolving time (CRT), nor the difference in the flight time of the prompt gamma and annihilation photons before they are detected. In this paper, we develop a statistical framework for lifetime image reconstruction. Our work formulates a statistical model for the PLI list-mode events considering the limited TOF resolution. The framework does not require precise knowledge of the radiotracer distribution, nor the direct measurement of the time delay between the prompt gamma and the annihilation photons, which inevitably includes the effects from finite CRT. A compute-efficient gradient-descent algorithm is developed to solve for the maximum-likelihood (ML) solution according to this statistical model. Using simulated list-mode data derived from numerical phantoms, we find that our framework and algorithm can quantitatively recover the lifetime image, subject to variability due to noise.

The remainder of this paper is organized as follows. Section II formulates the statistical model for observing the PLI list-mode events from which maximum likelihood estimations are derived for the reconstruction of both radiotracer activity and lifetime maps. Section III presents the phantom study of the proposed reconstruction methods including the generation of list-mode PLI events using Monte-Carlo simulation as well as the lifetime image reconstruction from the PLI events. Comparisons between our reconstruction and backprojections using the most-likely position from TOF highlight the performance benefit of our method under finite CRT. Section IV provides a summary and conclusion.

II. STATISTICAL MODEL FOR POSITRONIUM LIFETIME IMAGING

The concept of PLI is illustrated in Figure II. PLI uses the same scanner geometry as conventional TOF PET which is a ring of detectors uniformly spaced on the gantry. Contrary to the radiotracer used in traditional PET, PLI uses an isotope, such as Sc-44, that emits a prompt gamma photon as soon as a positron is released. Suppose an isotope decay occurs at location \mathbf{r}_{decay} . The prompt gamma may travel from \mathbf{r}_{decay}

Z. Zhu, C. Harrison and H.-H. Huang are with the University of Central Florida and C.-M. Kao is with the University of Chicago.

towards the detector gantry at a random direction, denoted by the angle ϕ_γ , and detected by the detector i_γ which is shown as the blue line in the figure. Meanwhile, the positron forms positronium with the surrounding electrons before it annihilates into a pair of 511keV gamma photons. The time between the formation and annihilation of the positronium, denoted by τ , is its lifetime. Interactions between positronium and the surrounding environment shortens its lifetime which reflects the concentration of paramagnetic molecules such as oxygen.

The 511keV gamma photon pair emitted from positronium annihilation travels from \mathbf{r}_{decay} towards random but opposite directions ϕ_{511keV} before reaching a pair of detectors, denoted by the indexes $i_{511keV,1}$ and $i_{511keV,2}$, on the gantry. The difference in time-of-flight (TOF) between the 511keV gamma photon pair Δt_{511keV} is measured. The detection process of the 511keV annihilation pair is similar to that in traditional TOF PET. The three measurable event attributes, $i_{511keV,1}$, $i_{511keV,2}$, and Δt_{511keV} , constitute the TOF PET coincidence channel c . The former two determine the line of response (LOR) along which the 511keV annihilation photon pair is detected, and the third attribute is determined by the location \mathbf{r}_{decay} along the LOR as well as the system CRT. On top of the coincidence channel c , each PLI event $w = (c, i_\gamma, \Delta t_\gamma)$ also includes the detector that receives the prompt gamma i_γ and the time difference Δt_γ between the detection of prompt gamma and annihilation pair. It is worth noting that Δt_γ is not a direct measurement of the positronium lifetime since it includes the effects from the travel times of prompt gamma and the annihilation pair as well as the finite CRT of the system.

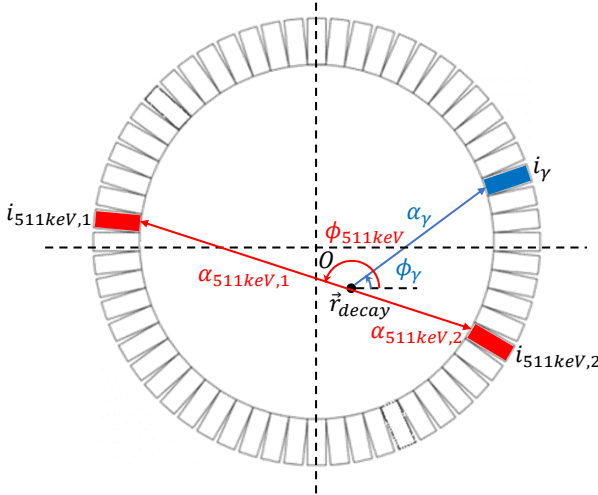


Fig. 1. Illustration of the setup and event detection in positronium lifetime imaging.

In tissue, a considerable amount of the released positrons forms ortho-positroniums (oPs) that can remain stable for a sufficiently long period to allow their positrons to interact with the environment and annihilate, shortening their lifetime in vacuum. Hence, the oPs' lifetime in tissue reflects the property of their environment. This is a stochastic process: the observed time τ between creation of the positroniums, which happens almost instantaneously after isotope decay, and the

annihilation can be described by an exponential distribution $\lambda \exp(-\lambda \tau)$, where the reciprocal of the rate constant λ is the mean lifetime time. Let λ_j and f_j denote the rate constant and PET isotope concentration within image voxel j , respectively. The probability of observing the k -th PLI event falling into the TOF coincidence channel c_k and having lifetime τ_k follows a mixture of exponential distributions,

$$p(\{c_k, \tau_k\} | \boldsymbol{\lambda}; \mathbf{f}) = \sum_{j=1}^J H_{c_k, j} f_j \lambda_j \exp(-\lambda_j \tau_k), \quad (1)$$

where each element in the system matrix, $H_{c, j}$, denotes the probability for an annihilation pair in voxel j to be detected by TOF channel c . Previously, the elements in system matrix \mathbf{H} are constructed from the multi-ray tracing method [6] by calculating the length of each LOR segment, defined by the line connecting $(i_{511keV,1}, i_{511keV,2})$ and the timing bin width of Δt_{511keV} , intersecting each voxel. We construct \mathbf{H} by examining all the channels responding to an event from voxel j . Given the finite CRT, each voxel j contributes to a series of TOF channels $c_m = (i_{511keV,1}, i_{511keV,2}, \Delta t_{511keV, m})$, $m = 1, 2, \dots$, which share the same attributes $i_{511keV,1}$ and $i_{511keV,2}$ while differing in the attribute Δt_{511keV} , according to a Gaussian function

$$H_{c_m, j} = \exp(-(\Delta t_{511keV, j} - \Delta t_{511keV, m})^2 / (2\sigma_t^2)), \quad (2)$$

where $\Delta t_{511keV, j}$ is the accurate TOF value of voxel j reaching detectors $(i_{511keV,1}, i_{511keV,2})$, $\Delta t_{511keV, m}$ is the center of the timing bin in channel c_m , and the standard deviation of the Gaussian function is related to the CRT via $\sigma_t = CRT / (2\sqrt{2 \ln 2})$. We also normalize \mathbf{H} so that $\sum_c H_{c, j} = 1$ (i.e. all the events from each voxel are detected). The log-likelihood yields

$$l(\boldsymbol{\lambda}, \mathbf{f} | \{i_k, \tau_k\}) = \sum_{k=1}^N \log \left(\sum_{j=1}^J H_{c_k, j} f_j \times \lambda_j e^{-\lambda_j \tau_k} \right). \quad (3)$$

From Equation (1), we can derive the marginal probability by integrating over λ ,

$$p(\{c_k\} | \mathbf{f}) = \prod_k \left(\sum_j H_{c_k, j} f_j \right). \quad (4)$$

where we have used $\int \lambda \exp(-\lambda \tau) d\lambda = 1$ to derive the conventional TOF likelihood function. The marginal log-likelihood of observing the k -th PLI event at coincidence channels $\{c_k\}$ is thus

$$l(\mathbf{f} | \{c_k\}) = \sum_k \log \left(\sum_j H_{c_k, j} f_j + \varepsilon \right), \quad (5)$$

which shares the same form as the Poisson log-likelihood if we aggregate the number of counts within each coincidence channel c_k . Here we have included a small number $\varepsilon = 10^{-8}$ to prevent the singularity in the logarithm function.

The activity map \mathbf{f} and rate-constant map $\boldsymbol{\lambda}$ can be jointly estimated from the log likelihoods using gradient-based optimizations. The gradient of $l(\boldsymbol{\lambda}, \mathbf{f} | \{i_k, \tau_k\})$ (see Equation (3)) with respect to $\boldsymbol{\lambda}$ is given by the following:

$$\frac{\partial l(\boldsymbol{\lambda}, \mathbf{f})}{\partial \lambda_j} = \sum_{k=1}^N \frac{H_{c_k, j} f_j (1 - \tau_k \lambda_j) e^{-\lambda_j \tau_k}}{\sum_{j=1}^J H_{c_k, j} f_j \times \lambda_j e^{-\lambda_j \tau_k}}. \quad (6)$$

TABLE I
DISTRIBUTION OF INDEPENDENT EVENT ATTRIBUTES IN THE
MONTE-CARLO SIMULATION

Unobservable attribute	Distribution
t_{decay}	$\mathcal{U}_{[0,T]}$
ϕ_γ	$\mathcal{U}_{[0,2\pi]}$
τ	$\lambda \exp(-\lambda \tau)$
ϕ_{511keV}	$\mathcal{U}_{[0,2\pi]}$

The gradient of $l(\mathbf{f}|\{i_k\})$ (see Equation (5)) with respect to \mathbf{f} can be derived as

$$\frac{\partial l(\mathbf{f})}{\partial f_j} = \sum_k \frac{H_{c_k,j}}{\sum_j H_{c_k,j} f_j + \varepsilon}. \quad (7)$$

Our proposed statistical reconstruction method starts with uniform initial guesses for both $\hat{\mathbf{f}}$ and $\hat{\boldsymbol{\lambda}}$. We first perform reconstruction on \mathbf{f} , which updates the solution at the n -th iteration using

$$\hat{\mathbf{f}}_{n+1} = \hat{\mathbf{f}}_n - \eta_f \times \left. \frac{\partial l(\mathbf{f})}{\partial \mathbf{f}} \right|_{\hat{\mathbf{f}}_n}. \quad (8)$$

Given the reconstructed $\hat{\mathbf{f}}$, we then perform iterations to reconstruct $\hat{\boldsymbol{\lambda}}$ using

$$\hat{\boldsymbol{\lambda}}_{n+1} = \hat{\boldsymbol{\lambda}}_n - \eta_\lambda \times \left. \frac{\partial l(\mathbf{f}, \boldsymbol{\lambda})}{\partial \boldsymbol{\lambda}} \right|_{\hat{\mathbf{f}}, \hat{\boldsymbol{\lambda}}_n}. \quad (9)$$

Here both the step sizes η_λ and η_f are empirically determined to be 0.0002.

III. SIMULATION

A. List-mode event generation

The list mode events $W = \{w_k, k = 0, 1, 2, \dots, (K - 1)\}$ can be simulated using Monte-Carlo methods under a small-animal PET geometry. Each event word w_k stores the observable attributes, $(c_k, i_{\gamma k}, \Delta t_{\gamma k})$, where $c_k = (i_{511keV,1,k}, i_{511keV,2,k}, \Delta t_{511keV,k})$ denotes the TOF coincidence channel, i_γ is the detector that receives the initial gamma ray photon, and Δt_γ is the time difference between the isotope decay and the observed annihilation photon pair. If the distance traveled by the positron from the location of isotope decay to that of annihilation is negligible, Δt_γ can be considered as a biased observation of the positron lifetime τ . The event words are generated from the independent but unobservable attributes $(t_{decay}, \phi_\gamma, \tau, \phi_{511keV})$. Here t_{decay} is the start time of the initial decay event within the observation time window $[0, T]$, ϕ_γ is the travel direction of the gamma ray photon at the start of the decay event, τ is the positronium lifetime after which a 511keV gamma ray photon pair is produced from the annihilation of the positron, and ϕ_{511keV} is the travel direction of the 511keV gamma ray photon pair. Table III-A summarizes the distribution from which all observable attributes are generated from the Monte-Carlo simulation.

The scanner consists of N_{det} detectors uniformly spaced in the angular range $(0, 2\pi)$ on the gantry with diameter D . For each pixel (i, j) in the object, $\mathbf{r}_{decay} = (x_{decay}, y_{decay})$ falls within $[x_i : x_i + \Delta x, y_j : y_j + \Delta y]$, where Δx and Δy are the pixel size along the x and y directions, respectively. Given the travel

direction of the gamma ray photon ϕ the distance α it travels before reaching the gantry satisfies a quadratic relation:

$$|\mathbf{r}_{decay} + \alpha(\cos \phi, \sin \phi)| = D/2. \quad (10)$$

Equation (10) yields two solutions:

$$\alpha_\pm(\phi) = -(x_{decay} \cos \phi + y_{decay} \sin \phi) \pm \sqrt{(x_{decay} \cos \phi + y_{decay} \sin \phi)^2 - (x_{decay}^2 + y_{decay}^2 - D^2/4)} \quad (11)$$

with the positive and negative solutions pointing toward and opposite the direction of travel, respectively. For the initial gamma ray photon, we set $\phi = \phi_\gamma$, and use only the positive solution α_+ to calculate $t_\gamma = t_{decay} + \alpha_+(\phi_\gamma)/c$ and i_γ . The negative solution is equivalent to choosing $\phi = \phi_\gamma + \pi$, and since ϕ_γ is uniformly distributed in $[0, 2\pi]$, choosing the positive solution here does not affect the distribution of the generated event attributes. For the 511keV annihilation photon pair, we set $\phi = \phi_{511keV}$, and both positive and negative solutions are used to calculate $t_{511keV,1}$, $t_{511keV,2}$, and c_{511keV} . The indexes of the detectors that receive the gamma ray photon are obtained from rounding the angular position of the photon event on the gantry:

$$i = \lfloor N_{det} \angle(\mathbf{r}_{decay} + \alpha(\cos \phi, \sin \phi)) / (2\pi) \rfloor \quad (12)$$

where $\lfloor x \rfloor$ denotes rounding to the nearest integer smaller than x . The arrival time of the two photons in the 511keV photon pair can be calculated as $t_{511keV,1} = t_{decay} + \tau + \alpha_+(\phi_{511keV})/v_c$ and $t_{511keV,2} = t_{decay} + \tau + \alpha_-(\phi_{511keV})/v_c$ respectively, where v_c is the speed of light. The difference between the arrival times of the gamma ray pair along LOR is

$$\Delta t = t_{511keV,1} - t_{511keV,2} = (\alpha_+(\phi_{511keV}) - \alpha_-(\phi_{511keV})) / v_c. \quad (13)$$

The time difference between the detection of the gamma ray photon from the initial isotope decay and the observed annihilation photon pair is

$$\Delta t_\gamma = (t_{511keV,1} + t_{511keV,2}) / 2 - t_\gamma = \tau + [(\alpha_+(\phi_{511keV}) + \alpha_-(\phi_{511keV})) / 2 - \alpha_+(\phi_\gamma)] / v_c. \quad (14)$$

To simulate the effect of finite CRT, we add random numbers drawn from a Gaussian distribution $N(0, \sigma_i)$ to both Δt_γ and Δt . After the temporal blurring, Δt_γ and Δt are stored as discrete bin indices with the bin size used in constructing the system matrix \mathbf{H} .

B. Reconstruction results

We generated the list-mode TOF events using Monte-Carlo simulations described in Sec. III. The scanner consisted of $N_{det} = 288$ detectors with a gantry diameter of $D = 57$ cm. The simulated CRT was 570 ps FWHM with 400 ps TOF bins. 14 TOF bins were used in the simulation, giving a total number of 1.16 million TOF coincidence channels. The images were represented by an array of $3.27 \text{ mm} \times 3.27 \text{ mm}$ square pixels.

Because Δt_γ is an indirect measurement of τ , we first estimated $\hat{\tau}_k$ using all five attributes of each event. Specifically, given the coincidence channel c_k , the overall length of the LOR, $\alpha_+ + \alpha_-$, can be obtained. Combined with the

TOF value Δt_k , both α_+ and α_- can be solved with errors comparable to $c \times \text{CRT}$. The $\hat{\tau}_k$ value of each event can then be estimated using Equation (14) and used in the log likelihood (see Equation (1)) for statistical reconstruction. For comparison, the rate-constant map was also estimated by backprojecting the events and then taking the average of $\hat{\tau}_k$ for each pixel:

$$\hat{\lambda} = \frac{\sum_k H_{i_k, j}}{\sum_k H_{i_k, j} \hat{\tau}_k}. \quad (15)$$

In the following discussions, we refer to the backprojection and maximum likelihood reconstruction methods as BP and ML, respectively.

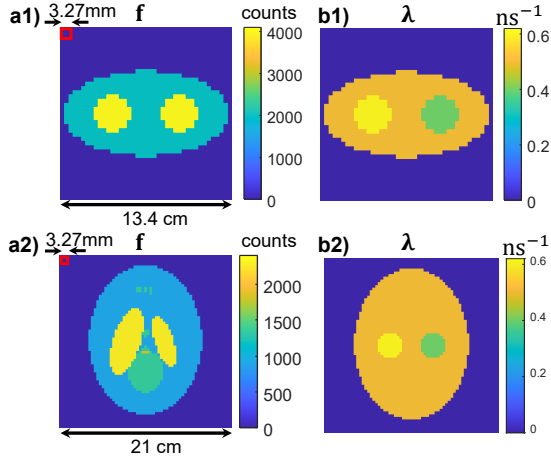


Fig. 2. 2D activity (a) and decay rate (b) of the two simulation phantoms.

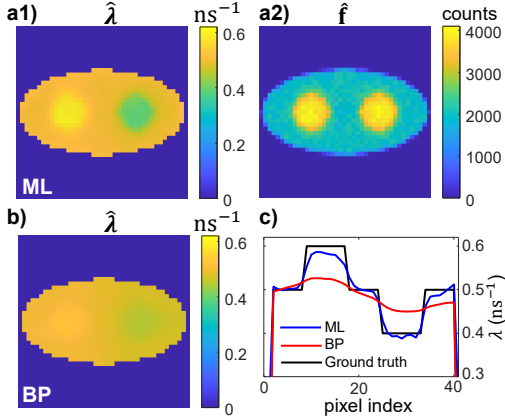


Fig. 3. Reconstructed rate-constant image of phantom 1 from (a) ML (also includes f in (a2)) and (b) BP. (c) Comparison of the horizontal profiles across the center of the rate-constant images.

We evaluated the performance of the proposed statistical reconstruction method on two phantoms. Fig. 2 shows the activity and rate-constant image phantoms in the simulation. Phantom 1 has a uniform elliptical activity map measuring 13.0 cm by 6.5 cm along the major and minor axes, respectively. The rate-constant image of phantom 1 contains two discs that have different λ values (0.4 and 0.6 ns^{-1}) from the background ellipse (0.5 ns^{-1}). A total number of 1.5 million events were generated in the Monte-Carlo simulation.

Phantom 2 is a modified Shepp-Logan pattern with a diameter of 21cm. The rate-constant image contains two discs of 3.2 cm in diameter with different λ values of 0.4 and 0.6 ns^{-1} from the background (0.5 ns^{-1}). The expected total number of events was 4 million for phantom 1 and 8 million for phantom 2. Neither attenuation nor scattering were included.

Fig. 3 compares the rate-constant images reconstructed from ML (Fig. 3(a1)) and BP (Fig. 3(b)). We quantify the reconstruction accuracy using the normalized mean square error (NMSE), defined as

$$\text{NMSE} = \frac{|\hat{\lambda} - \lambda|_2^2}{|\lambda|_2^2}. \quad (16)$$

Here $\hat{\lambda}$ and λ are the reconstructed rate-constant image and its ground truth, respectively, and $|\cdot|_2$ denotes the L2-norm. The TOF resolution of 570 ps translates into a spatial uncertainty of 8.5 cm, which is larger than half of the phantom dimension. As a result, BP produces a highly blurred rate-constant image. ML reconstruction, on the other hand, produces higher contrast between the active region and the background. Fig. 3(c) compares the horizontal profiles across the center of the reconstructed rate-constant images with the ground truth. The NMSEs of the rate-constant profiles are 3.1×10^{-5} and 2.4×10^{-4} , respectively, for ML and BP which indicates that ML produces a quantitatively better image quality than BP.

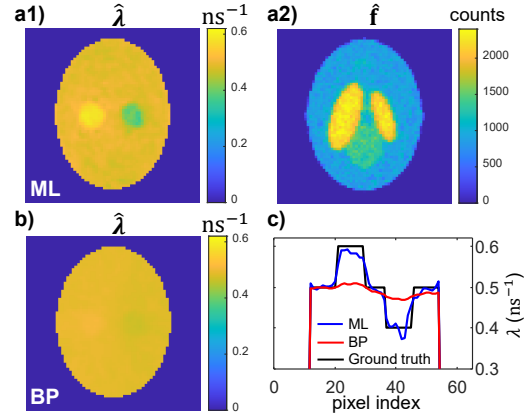


Fig. 4. Reconstructed rate-constant image of phantom 2 from (a) ML (also includes f in (a2)) and (b) BP. (c) Comparison of the horizontal profiles across the center of rate-constant images.

Figure 4 shows the ML reconstructions of activity and rate-constant maps for phantom 2. The NMSEs of the rate-constant profiles are 3.5×10^{-5} and 2.7×10^{-4} , respectively, for ML and BP, again quantitatively indicating better reconstruction from ML. The reconstructed rate-constant image exhibits little to no crosstalk with the activity map.

IV. SUMMARY AND DISCUSSIONS

We have demonstrated an ML algorithm for reconstructing positronium lifetime images from extended TOF PET data. Currently, the 64×64 phantom size is only limited by the available computing resources. The capability to perform high-resolution, high-fidelity lifetime image reconstruction on a scale of tens of centimeters with millimeter spatial resolution

suggests the feasibility of our method for small-animal PET scans.

The statistical reconstruction algorithm produces quantitatively correct lifetime images for a simulated 570ps TOF system. Observe that $\hat{\tau}_k$ estimated from Eq. (14) is not exact because both α_+ and α_- contain uncertainties due to the finite timing resolution of the system. Given the TOF resolution of 570 ps, the error in $\hat{\tau}_k$ is around 0.6 ns. In contrast, the positronium lifetime in our phantom has a mean of 2 ns. Because the error in $\hat{\tau}_k$ is small compared to the value of τ_k itself, ML results agree with the ground truth well. In the future, we will investigate formulating a likelihood function involving the observable $\Delta t_{\gamma k}$ in the maximum likelihood estimation of both \mathbf{f} and $\boldsymbol{\lambda}$.

REFERENCES

- [1] P. Moskal, D. Kisielewska, C. Curceanu, E. Czerwiński, K. Dulski, A. Gajos, M. Gorgol, B. Hiesmayr, B. Jasińska, K. Kacprzak *et al.*, “Feasibility study of the positronium imaging with the j-pet tomograph,” *Physics in Medicine & Biology*, vol. 64, no. 5, p. 055017, 2019.
- [2] P. Moskal, B. Jasinska, E. Stepien, and S. D. Bass, “Positronium in medicine and biology,” *Nature Reviews Physics*, vol. 1, no. 9, pp. 527–529, 2019.
- [3] K. Ote and F. Hashimoto, “Deep-learning-based fast tof-pet image reconstruction using direction information,” *Radiological Physics and Technology*, vol. 15, no. 1, pp. 72–82, 2022.
- [4] M. D. Harpen, “Positronium: Review of symmetry, conserved quantities and decay for the radiological physicist,” *Medical Physics*, vol. 31, no. 1, pp. 57–61, 2004.
- [5] J. Qi, “Positronium lifetime image reconstruction for tof pet,” *IEEE Trans Med Imag*, vol. In press, 2022.
- [6] R. H. Huesman, G. J. Klein, W. W. Moses, J. Qi, B. W. Reutter, and P. R. Virador, “List-mode maximum-likelihood reconstruction applied to positron emission mammography (pem) with irregular sampling,” *IEEE transactions on medical imaging*, vol. 19, no. 5, pp. 532–537, 2000.